ACS APPLIED ELECTRONIC MATERIALS

pubs.acs.org/acsaelm

Article

Solution-Processed Low Resistivity Zinc Oxide Nanoparticle Film with Enhanced Stability Using EVOH

Mengyang Qu,* Sheng Yong, Ben D. Rowlinson, Amanda A. Green, Stephen P. Beeby, Harold M. H. Chong, and Maurits R. R. de Planque

Cite This: *ACS Appl. Electron. Mater.* 2024, 6, 4277−4287

Read Online

ACCESS | Metrics & More | Article Recommendations | Supporting Information

ABSTRACT: This paper proposes a solution-based fabrication process of the zinc oxide nanoparticle (ZnO NP) film. It achieves a resistivity comparable to that of ZnO deposited by using physical and chemical vapor deposition methods. The process involves exposing the solution-processed ZnO NP film to 365 nm ultraviolet light and passivating it with an ethylene vinyl alcohol (EVOH) encapsulant of 80 μm under a vacuum. The manufacturing process has a maximum temperature of 190 °C, enabling use on flexible substrates, such as polyimide. The fabricated ZnO film has a sheet resistance of 2.5 × 10^4 Ω/□ and a thickness of 2.35 μm. The EVOH passivation layer enhanced the film stability, protecting it when exposed to the ambient environment. The resistivity of the ZnO NP layer with EVOH passivation remains unchanged after 60 days in an ambient environment.

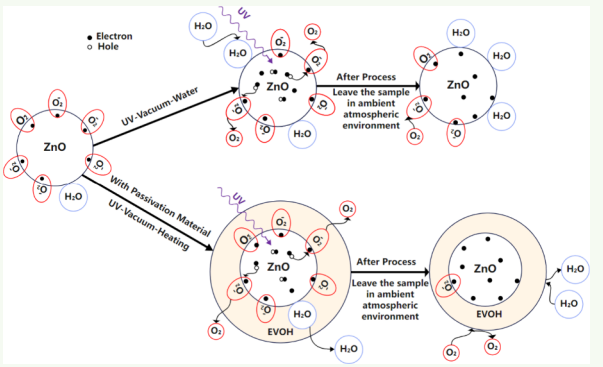

KEYWORDS: *solution-based process, ZnO nanoparticle, surface oxygen absorbance, low resistivity, electrical stability, surface passivation*

1. INTRODUCTION

Solution-processed functional films have been demonstrated in many applications, including the human−computer interface,[1] point-of-care equipment,[2,3] wearable devices,[4] and light-emitting devices.[5] These spin-coated or printed films have been utilized in numerous sensing applications, such as gas,[6] biomarkers,[7] and moisture.[8] A solution-processed deposition method at room temperature in ambient conditions offers a low-cost, low-temperature fabrication method with reduced environmental impact compared to a chemical or physical vapor deposition process.[9] These functional films are categorized into organic and inorganic materials; however, in this article, we focus on the fabrication of a solution-processed inorganic semiconductor layer.

Inorganic semiconductor materials, such as metal oxides, including indium oxide (In_2O_3),[10,11] indium zinc oxide (IZO),[12] indium gallium zinc oxide (IGZO),[13,14] and zinc oxide (ZnO),[15−20] are compatible with solution-based deposition manufacturing processes. For example, metal oxide precursors or particles would be added to a dispersion agent formulated to the correct rheology for printing[11,21,22] or spin coating[23,24] onto a substrate followed by a suitable drying/curing step to form the semiconductor layer. Semiconducting ZnO NP sensors that change resistance have gained widespread attention due to their low cost, high electron mobility, and robust chemical and thermal stability.[25] The predominant sensing mechanism by which the ZnO functional layers respond to a measurand is chemical surface adsorption.[25] For n-type ZnO NPs, the adsorption of chemical analytes on the nanoparticle's surface influences carrier binding or release, thereby modulating its resistance.[26] Oxygen molecules, for example, bind free electrons within ZnO NPs, forming highly active oxygen species, increasing the film resistivity.[26−29] The sensing mechanism within ZnO NPs for reducing substances is closely tied to surface oxygen, whereby reducing substances undergo oxidation by oxygen species, releasing trapped electrons and consequently reducing the resistivity of ZnO NPs.[26,27] Even with a low target molecule concentration of 1 ppm, chemiresistive sensors can exhibit a resistance change of over 50%.[26] Studies have indicated that chemical analytes are not required to be in direct contact with the ZnO surface; rather, deposition of a dielectric layer such as aluminum oxide, silicon oxide, or APTES on the ZnO surface allows analyte adsorption to alter ZnO resistance through a field effect.[30−33]

However, ZnO NP presents two primary drawbacks, high resistivity and susceptibility to environmental influences, resulting in the unpredictable electrical behavior of devices. Therefore, improving the ZnO device's electrical stability is critical in this research area.[34] While solution-processed metal

Received: February 26, 2024
Revised: May 16, 2024
Accepted: May 16, 2024
Published: May 30, 2024

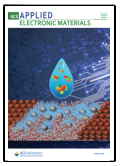

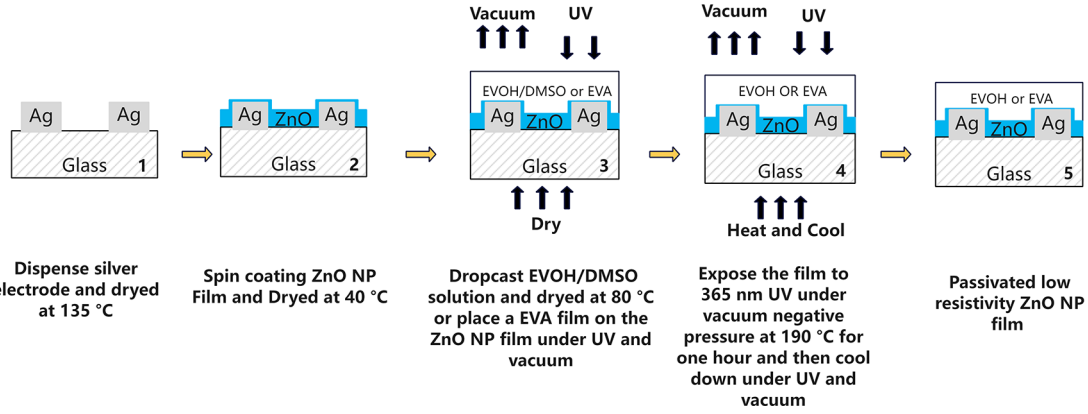

Figure 1. Schematic fabrication process flow for solution-based deposition of the ZnO NP device. Starting from the dispenser printing interdigitated silver electrode, spin coating of the ZnO NP layer. The fabrication process in step 3 is to dry DMSO/EVOH or hot-melt the EVA film. The EVOH solution is drop-cast, and the EVA film is directly applied on the ZnO surface. Step 4 shows the passivation treatment using EVOH and EVA polymers under the UV-vacuum-heat process for 1 h and then cooling down to room temperature under UV-vacuum condition.

oxide semiconductor materials are resilient to decomposition in ambient environments, their electronic properties remain susceptible to environmental influences.[35] Molecules from the ambient environment with weak hydrogen bonds can become dissociated, leading to electron binding within ZnO, influencing its resistivity.[36] Additionally, resistance measurements are likely conducted immediately after film deposition due to the propensity of ZnO film resistance to increase upon exposure to ambient conditions. Limited studies have explored the long-term stability of the electrical properties of ZnO NP films. According to the literature,[25,36−38] the elevated resistivity of ZnO NP correlates with oxygen molecules adsorbed on its surface, which diminishes the carrier concentration of ZnO NPs. While high-resistivity ZnO films exhibit improved semiconductor response rates, their electrical characteristics are more influenced by environmental factors such as light and moisture. To mitigate high resistivity and enhance electrical stability, UV light can temporarily revert adsorbed oxygen to the gas phase, facilitating its removal from the surface of ZnO NP films under negative pressure condition. After being stored in a dark environment, the resistivity of the samples would increase considerably.[39] Preventing oxygen readsorption requires the use of passivation layers composed of hydroxyl groups, such as water molecules.[24,28] Therefore, a passivation layer with low oxygen permeability and high thermal stability is essential to sustain low resistivity over time.

Several polymer passivation layers have demonstrated capability in meeting the aforementioned requirements,[40] with ethylene vinyl alcohol (EVOH) being particularly prominent. Ethylene vinyl alcohol (EVOH), derived from ethylene vinyl acetate (EVA),[41] serves as a widely utilized flexible oxygen barrier in various applications,[41−43] including its role as an airtight encapsulant for sensitive electronic materials. This polymer film finds extensive use as a passivation layer in electrical applications, including solar cells,[44,45] supercapacitors,[46] and thin film transistors.[47] EVOH is an environmentally friendly, durable, and a low-toxicity polymer that can be used as a cost-effective gas barrier material.[41−43] The presence of hydroxyl functional groups within its molecular structure enables facile adsorption onto the surface of ZnO NPs. Additionally, the oxygen permeability of the EVOH barrier films can be modulated by adjusting the deposition temperatures. Elevating the film temperature to within the range of 180−200 °C, where 200 °C represents the melting point, enhances the oxygen permeability of EVOH, allowing oxygen to escape from the ZnO film surface. After cooling, the film regains its exceptional oxygen barrier properties.

Therefore, in this article, we develop a novel solution-based fabrication process to passivate ZnO NP films that reduces film resistivity and enhances electrical stability. The method involves spin-coating ZnO NP onto a patterned silver electrode, followed by heating of the solution-processed ZnO NP film in a vacuum environment while continuously exposing it to ultraviolet (UV) light to eliminate the oxygen molecules. UV light aids in disrupting the bond between oxygen molecules and ZnO NP, while negative pressure aspiration and heating extract the oxygen molecules from the ZnO NP film. To assess the electrical stability of the ZnO NP films and prevent reabsorption of oxygen molecules, surface passivation is essential.[48] The passivation effect of water and polymers EVA and EVOH has been investigated. After 60 days, the resistivity of the ZnO NP film passivated with EVA and water molecules increased by a factor of 10^6, while the resistivity of ZnO NP passivated with EVOH only doubled. Re-exposing the films to UV light in an atmospheric environment achieves a 10^4 order of magnitude reduction in resistance for films passivated with EVA and water molecules, whereas films passivated with EVOH experience only a 20% reduction in resistivity.

2. METHODS

2.1. Material Preparation. In Zhang's study,[49] it was observed that a mixture of ZnO NPs with sizes ranging between 20 and 100 nm exhibited enhanced absorption of incident UV light, leading to increased removal of oxygen. In this work, two sizes of ZnO NPs (100 nm-diameter NP from Merck and 20 nm-diameter NP from Thermo Scientific) were blended in a ratio of 1:1 by weight and 0.205 g of the blended particles was dissolved in 1.6 mL of methanol (CH_4O, 99.8% from Merck). The solution was sonicated for 1 h and then stored in a refrigerator at 4 °C to reduce precipitation effects due to solvent volatilization. Fabinks TC-C4007 silver ink was used as the device electrode. For the EVOH passivation solution, 1 g of poly(vinyl alcohol-*co*-ethylene) (PVA-*co*-PE) with 32 mol % ethylene (Merck) and 10 mL of dimethyl sulfoxide (DMSO from Merck) was stirred and heated at 80

https://doi.org/10.1021/acsaelm.4c00355
ACS Appl. Electron. Mater. 2024, 6, 4277−4287

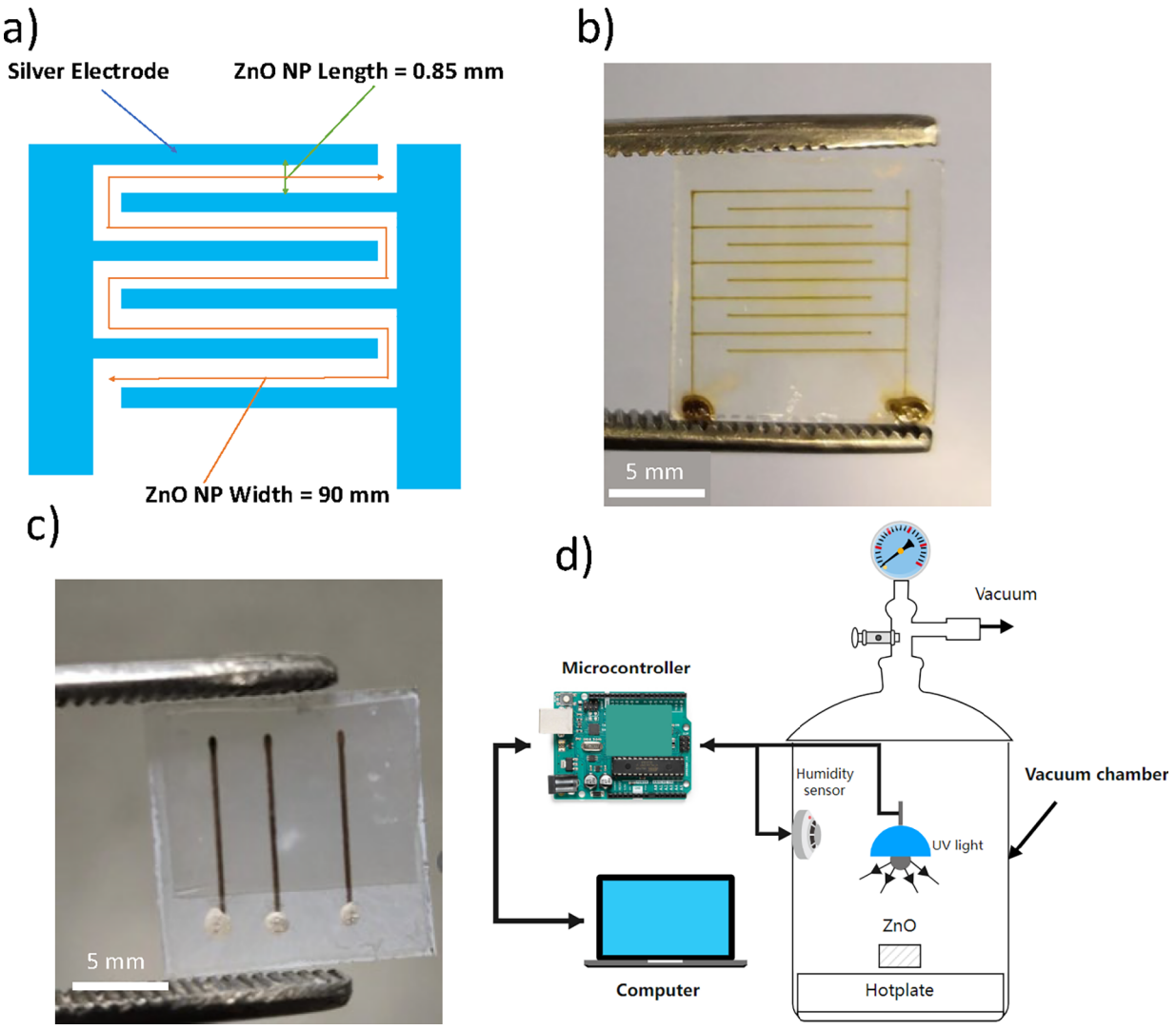

Figure 2. (a) Geometry design parameter of the interdigitate electrode device and the length and width of the ZnO NP film. (b) ZnO NP film with an interdigitated silver electrode after UV-vacuum-heat EVOH passivation. The effective electrode channel width is 90 mm, and the length is 0.85 mm. (c) TLM structure with the gaps between lines of 4 and 6 mm and passivated by EVA. (d) Schematic diagram of the vacuum ultraviolet light exposure system. The UV light and humidity sensor inside the vacuum box are controlled by a microcontroller. An external power supply controlled the hot plate.

°C on the hot plate under vacuum conditions for 4 h. The EVOH solution was applied directly onto the ZnO film during the fabrication process. For the EVA film fabrication, 0.6 g of poly(ethylene-*co*-vinyl acetate from Merck) with 12 wt % vinyl acetate stock was soaked in 6 mL of trichlorobenzene for 1 day. Then, the mixture was speed-mixed at 3000 rpm for 1 min and heated at 100 °C in a water bath. After the solution was fully mixed, it was drop-cast onto a glass substrate and heated at 135 °C in the box oven for 1 h to dry the film. After cooling, the film was peeled from the glass and applied as a dry film to ZnO where it is heated to 190 °C, which bonds it to the surface of the ZnO NP film. The influence of water molecules was investigated by increasing the humidity within the chamber during the UV exposure.

2.2. Fabrication Process. The fabrication process is illustrated in Figure 1. The TC-C4007 silver ink was speed-mixed at 3000 rpm for 1 min and then printed on a 15 mm × 15 mm glass slide using a Fisnar F7300NV dispenser printer. There were two silver electrode patterns printed on the glass. First, to test the time-dependent stability, an interdigitated electrode structure was used, with an effective channel width (W) and length (L) as shown in the schematic diagram (Figure 2a,b) with a W/L ratio of 90 ± 5 mm:0.85 ± 0.06 mm = 105. For the transfer length method (TLM), six 10 mm-long, 0.25 mm-wide lines were printed on the glass with the distance between the adjacent lines being 2, 4, 6, 8, and 10 mm. Figure 2c shows the TLM lines with 4 and 6 mm wide spacing. These films were used for measuring the contact resistance, sheet resistance, and transfer length. Then, ZnO thin films were formed by a spin-coating process at 2000 rpm for 20 s upon the silver contact electrodes. The samples were then dried on a hot plate at 40 °C for 5 min.

For the study of water molecular interactions, the setup and process are shown in the Supporting Information (Figures S1 and S2); 10 mL of deionized water was placed in the beaker next to ZnO, and then both were heated under vacuum. When the relative humidity reached 70%, the 365 nm UV lamp was turned on for 1 h of exposure. The equipment for the UV-vacuum-heat fabrication process is shown in Figure 2d. The UV light intensity was set to 300 mW/cm^2. For the study of

https://doi.org/10.1021/acsaelm.4c00355
ACS Appl. Electron. Mater. 2024, 6, 4277−4287

EVA passivation, the EVA film was cut into a size of 13 mm × 15 mm and placed on top of the ZnO film. It was then subjected to vacuum (10^{-2} mbar) under ultraviolet light and heated to 190 °C for 1 h. For EVOH passivation, a 20−150 mL EVOH/DMSO solution was drop-cast onto the surface of the ZnO NP. The sample was then placed in the vacuum ultraviolet exposure equipment and heated to 80 °C for 1 h to remove the DMSO solvent, after which the sample was heated to 190 °C for 1 h. During the UV-vacuum-heat process, the vacuum pump was kept turned on to generate a negative pressure. EVA passivation layers can absorb 85% of the 365 nm wavelength UV light,[50] and EVOH passivation can absorb 50%.[51] Finally, the sample was allowed to cool to room temperature while still being exposed to the UV light under vacuum.

2.3. Measurement. To avoid the influence of ambient light, all ZnO NP samples were stored in the dark at room temperature and measurements were performed in a dark setting. The resistance of the thin film was measured by using a Keithley 2636B and Keysight B1500A source measurement unit with a Polytec MSA-400 MEMS probe station. The SEM image was taken using a Zeiss NVision 40 system. The resistance of the ZnO film was also measured by depositing the layers onto an interdigital electrode array, and the resistance of the device was determined by ZnO film resistivity.

For the calculation of the sheet resistance derived from an interdigitated device, the resistivity and sheet resistance of the material can be written as[52]

$$\rho = \frac{RA}{L} \tag{1}$$

$$R_{\text{sheet}} = \frac{\rho}{t} = \frac{RA}{Lt} = \frac{RWt}{Lt} = \frac{RW}{L} \tag{2}$$

where ρ and R_{sheet} represent the resistivity and sheet resistance, and A, W, t, and L represent the material area, width, thickness, and length, respectively. The active channel geometry is shown in Figure 2a, which is derived from Tyrrell et al.'s work.[53] The specific length and width are shown in Figure 2a. R is the measured resistance of the device.

The TLM structure, which is another way to calculate sheet resistance, is used to verify the sheet resistance calculation, and the equation is shown below:

$$R_{\text{total}} = \frac{R_{\text{sheet}}}{W}(2L_{\text{T}} + L) \tag{3}$$

where R_{total} is the measured resistance. The transfer length, L_{T}, is the average distance of the carrier traveling through the semiconductor under the contact before running up to the contact, and L is the length of the semiconductor.

3. RESULTS AND DISCUSSION

Electrical results were obtained from two samples with 5 measurements taken from each, unless otherwise stated. All of the figures show the average value. Figure 3 shows the scanning electron microscopy (SEM) image of the ZnO NP film with a thickness of 2.35 μm and its porous form. Figure 4a shows the resistance values of the interdigital device with the unprocessed ZnO NP film obtained for different UV-vacuum-heating processing times with measurements taken immediately after the process. The initial resistance of the unprocessed film was 200 MΩ but dropped to 5 kΩ after 10 min and dropped further to 1.3 kΩ after 60 min. Figure 4b summarizes the ZnO sheet resistance under different EVOH thicknesses after 1 and 60 days. With a thinner EVOH film (10 to 40 μm), the sheet resistance was significantly increased after 60 days but, for 80 μm EVOH film passivation, the sheet resistance was stable.

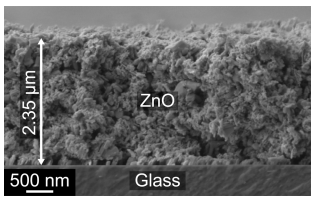

Figure 3. Cross-sectional SEM image of the solution-processed ZnO NP film on a glass substrate.

Figure 5 shows the change in ZnO sheet resistance over time calculated from the results of the interdigitated device. The W/L ratio of the ZnO NP film is 105, and its film sheet resistance is calculated from $R_{\text{sh}} = R \times W/L$, where R is the measured resistance. The 10−80 μm EVOH represents different passivation film thicknesses. The thickness of the EVA film is 0.8 mm. All of the passivation processes are under combined UV-vacuum-heating condition. The water molecule-passivated ZnO film had a sheet resistance of 0.21 MΩ/□ immediately after processing, which increased to 10 GΩ/□ after 1 day and finally settled at 20 GΩ/□. The resistance of the device passivated by EVA was initially around 42 kΩ/□, and this settled to 5 GΩ/□ after 3 days. The initial resistances of EVOH-passivated ZnO films are 14, 12, 31, and 68 kΩ/□ for EVOH thicknesses of 10, 20, 40, and 80 mm, respectively. After 60 days, these values had increased to 4.0 GΩ/□, 2.6 GΩ/□, 7.8 MΩ/□, and 13 kΩ/□, respectively. Table 1 summarizes the response of all devices following re-exposure to 365 nm UV light after 60 days. The resistance of the devices with water passivation and EVA passivation decreased by 10^4 times after being irradiated by UV light for 10 s. Devices passivated with EVOH are less responsive to UV exposure. The sheet resistance would decrease by a factor of 1000 for an EVOH thickness of 10 to 20 μm. However, the sheet resistance of EVOH thicknesses of 40 and 80 μm is reduced by factors of 50 and 1.4, respectively. The negligible resistivity change in the device with the 80 μm-thick passivation layer is due to the lack of adsorbed oxygen molecules on the surface of the ZnO NP film. This can be attributed to the thicker EVOH film, reducing the UV absorption on the ZnO film.

The sheet resistance of the unprocessed ZnO film (without the UV-vacuum-heat process) taken by TLM immediately after deposition (see Figures S3−S6) was 12 GΩ/□, and the contact resistance was 100 MΩ. The processed ZnO with water molecule passivation had a sheet resistance of 9 MΩ/□ and a contact resistance of 0.2 MΩ. The processed ZnO with EVA passivation exhibited a sheet resistance of 30 kΩ/□ and a contact resistance of 0.6 kΩ. The processed ZnO with 10 μm-thick EVOH passivation had a sheet resistance of 25 kΩ/□ and a contact resistance of 0.5 kΩ. These results show broad agreement with the resistivity measurements obtained from the interdigital devices (see Table 1).

It has been observed that reducing the oxygen partial pressure during the fabrication process increases the conductivity of ZnO. This can be due to the lower oxygen partial pressure, resulting in more oxygen vacancies in the ZnO lattice structure. Oxygen vacancies have long been considered to be one reason why ZnO exhibits n-type semiconducting properties.[54] The calculation based on first principles shows

https://doi.org/10.1021/acsaelm.4c00355
ACS Appl. Electron. Mater. 2024, 6, 4277−4287

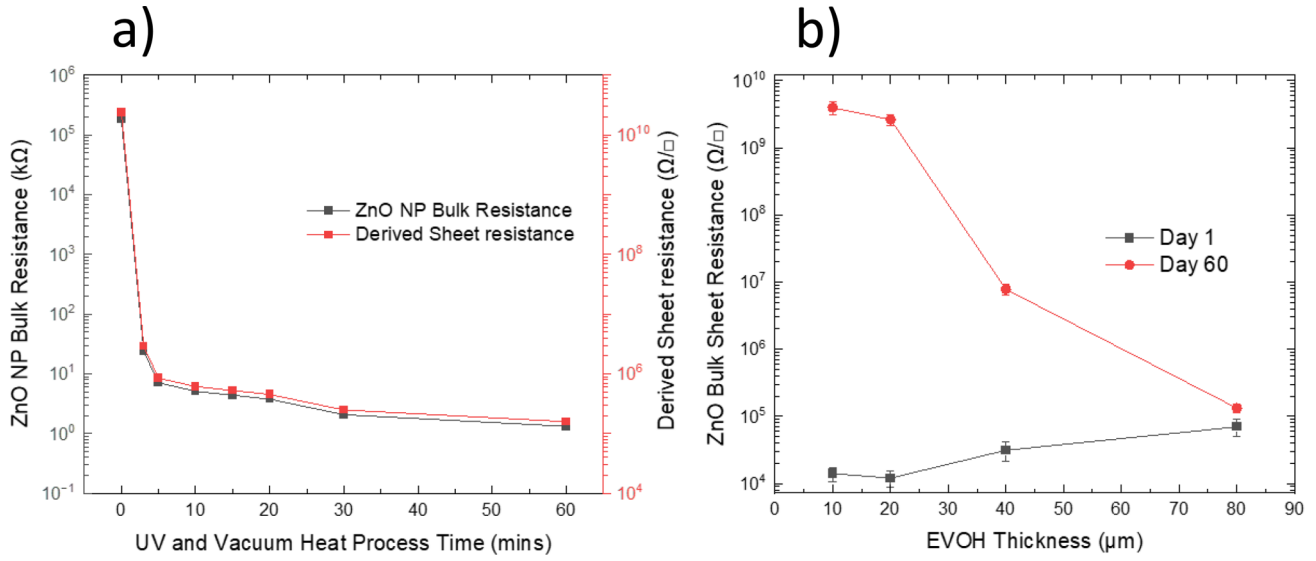

Figure 4. (a) Resistance of the interdigitated device without any passivation obtained after different UV-vacuum-heating times. The samples were exposed to the 365 nm-wavelength UV and heated to 190 °C in a 10^{-2} mbar vacuum condition. (b) ZnO NP bulk sheet resistance with different EVOH passivation thicknesses measured on day 1 and day 60. The lines joining the dots are guides for the eye, showing the change in bulk and sheet resistance with time and EVOH thicknesses.

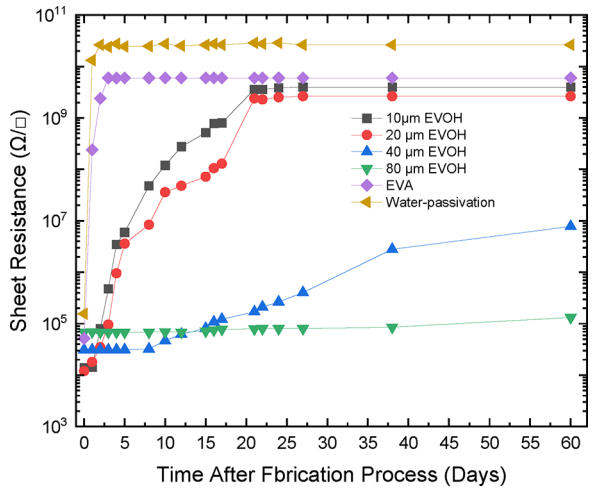

Figure 5. Measured time-dependent sheet resistance changes. The sheet resistance is calculated from the measured resistance of the device to its W/L ratio (Figure S7). The lines joining the dots are only guides for the eye.

Table 1. Resistance Response for 365 nm UV Interdigitated Devices Stored for 60 days in the Darkness after Processing

Interdigitated devices with different passivation	Initial ZnO sheet resistance after processing (Ω/□)	ZnO sheet resistance after 60 days stored in darkness (Ω/□)	Sheet resistance after re-exposure to 30 mW/cm^2 UV for 10 s (Ω/□)
10 μm EVOH	1.03×10^4	4.64×10^9	3.91×10^6
20 μm EVOH	1.23×10^4	3.26×10^9	1.93×10^6
40 μm EVOH	2.31×10^4	2.21×10^6	4.31×10^5
80 μm EVOH	6.00×10^4	1.11×10^5	0.88×10^5
EVA	4.56×10^4	5.78×10^9	1.82×10^5
Water passivation	6.31×10^4	2.42×10^{10}	6.08×10^6

that oxygen vacancies are located at very deep energy levels, are not shallow donors, and cannot therefore provide n-type conduction.[54,55] However, recent research shows that the oxygen vacancies on the surface of the ZnO NP easily absorb the oxygen molecule from the ambient environment and then trap the electron in the nanoparticle.[25]

According to the theoretical model proposed by Saputro et al.,[25] the ZnO surface with oxygen vacancies, or zinc oxygen dimer vacancies, can quickly adsorb oxygen molecules and convert them into two individual oxygen atoms. The oxygen atoms will trap the free electron and become oxygen ions, thereby reducing the carrier concentration inside the ZnO film and increasing its resistivity.

Experiments investigating the electrical characteristics of nano-ZnO under UV light exposure and in the presence of water have yielded a consistent hypothesis in which oxygen molecules adhere to the ZnO NP, binding with electrons.[36−38] Ultraviolet (UV) light can transiently release ionized oxygen molecules from the surface of ZnO NPs, thereby increasing the majority carrier concentration with water molecules, facilitating the maintenance of this concentration. The following equation can be used to define this phenomenon[36−38]

$$O_2(g) + e^- \rightarrow O_2^-(ad) \quad (4)$$

$$h\nu \rightarrow e^- + h^2 \quad (5)$$

$$O_2^-(ad) + h^+ \rightarrow O_2(g) \quad (6)$$

$$H_2O + 2Zn + O_V \rightarrow 2(Zn - OH) + V_o + 2e^- \quad (7)$$

where $O_2(g)$ and $O_2^-(ad)$ are the oxygen molecule in the gas phase and the adsorbed oxygen molecule on the ZnO surface, respectively, $h\nu$ is the UV energy, and e^- and h^+ are the electron and hole, respectively. O_V is the oxygen in the lattice, Zn−OH represents the zinc atoms with adsorbed hydroxyl groups, and V_o represents the oxygen vacancy. When ZnO is exposed to ultraviolet light, its internal electrons transition and leave holes in the valence band, forming electron−hole pairs. The formed holes migrate to the ZnO surface and neutralize the electrons bound by the oxygen molecules, thereby releasing the oxygen molecules and leaving behind the electrons that have transitioned. The carrier concentration increases accord-

https://doi.org/10.1021/acsaelm.4c00355
ACS Appl. Electron. Mater. 2024, 6, 4277−4287

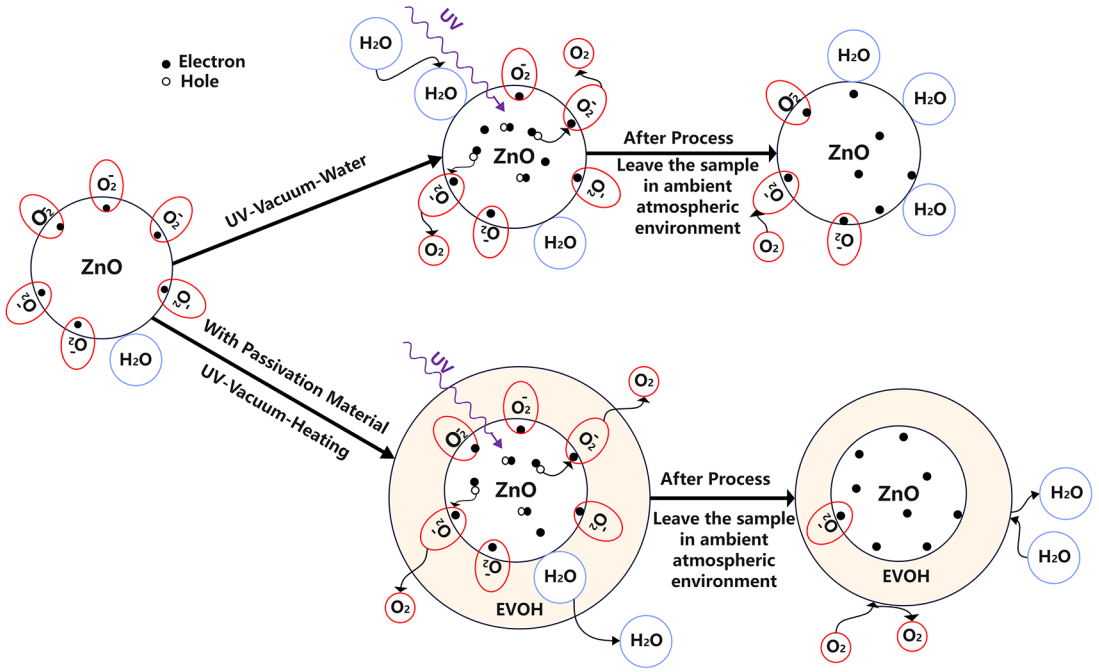

Figure 6. Schematic diagram of the release of carriers bound by oxygen on the ZnO surface by UV exposure in vacuum condition. The top path (derived from the literature[26,27,38]) shows the interaction of water molecules attached to the surface of the nanoparticles, and after leaving in ambient atmospheric condition, the oxygen molecules readily reabsorbed on the surface of ZnO. The bottom path shows the polymer passivation material (EVOH) that is more effective in preventing oxygen from being readsorbed.

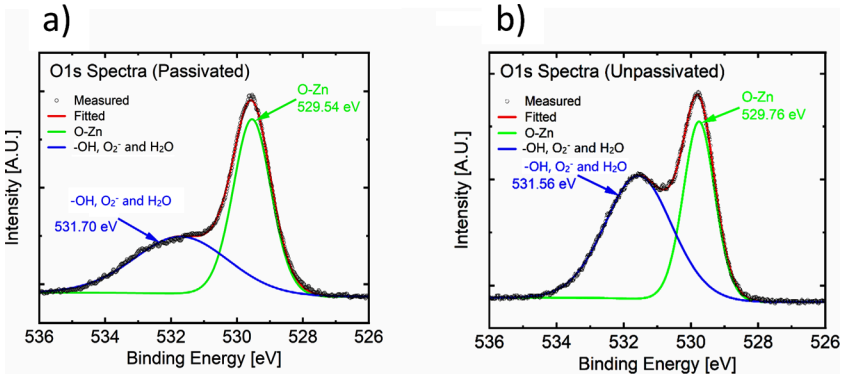

Figure 7. Measured O 1s XPS spectra of the ZnO NP film, (a) with EVOH passivation and the UV-vacuum-heat process and (b) without passivation and the UV-vacuum-heat process.

ingly, and the resistivity of ZnO decreases macroscopically. When the UV exposure is stopped, the oxygen molecules in the ambient environment will combine on the surface of ZnO to begin to reduce the carrier concentration again. Vidor et al.[38] show that if ZnO is exposed to a higher relative humidity environment, the resistance of ZnO will decrease significantly. After exposure to UV and moisture, if it is stored in a high humidity environment, the ZnO NP film will maintain a greater carrier concentration and lower resistance than a device stored in a dry environment.[38] This is due to the water molecules adsorbed on the surface of ZnO, which reduce the number of oxygen molecules adsorbed on its surface. However, the water molecules cannot be easily retained on the surface of ZnO and will evaporate unless high environmental humidity prevents this.

Figure 6 presents the schematic diagram explaining the impact of ZnO NP surface exposure to 365 nm UV radiation in vacuum condition, as described from the literature.[26,27,38] The released oxygen molecules in the gas phase diffuse into the environment. In this process, applying heat enhances the release rate of oxygen molecules.

The presence of the vacuum diminishes the concentration of released oxygen molecules on the ZnO NP surface. Figure 6 also illustrates the transient use of water molecules as a passivation layer on the ZnO NP surface; however, this effect is short-lived as the water molecules evaporate, leading to oxygen readsorption. The lower path in Figure 6 illustrates the application of EVOH polymer passivation to prevent oxygen molecule readsorption, preserving the ZnO electron concentration. In addition, the passivation layer with a lower oxygen permeability maintains the higher ZnO electron concentration for a longer duration. Regarding the effect of water molecules on the conductivity of the ZnO film, Liau and Lin[56] also proposed that water molecules will be dissociated into hydroxyl groups after contacting and adsorption on the ZnO film surface and increase the electron concentration.[56] The

https://doi.org/10.1021/acsaelm.4c00355
ACS Appl. Electron. Mater. 2024, 6, 4277−4287

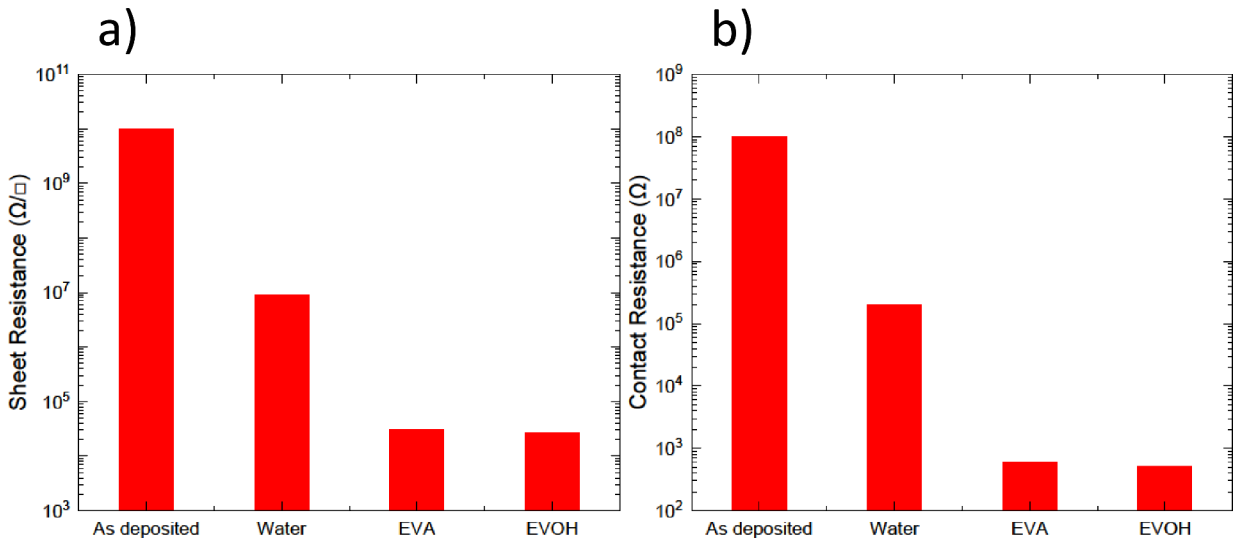

Figure 8. (a) Sheet resistance and (b) contact resistance results extracted from TLM measurement.

research of Rawal et al. on the interaction between water molecules and ZnO NP proposed that the dangling bonds that exist on the surface of ZnO NP will dissociate the adsorbed water molecules.[57]

To further understand the effect of oxygen and hydroxyl from water molecules, we have performed X-ray photoelectron spectroscopy (XPS) on both EVOH-passivated and non-passivated ZnO NP surfaces. The XPS measurement process is described in the Supporting Information. The deconvoluted core level O 1s spectrum in Figure 7a for a nonpassivated EVOH sample shows a distinct primary peak at 529.76 eV, characteristic of the O−Zn bond. A secondary peak at 531.56 eV is attributed to a combination of surface O_2^-, H_2O, and −OH hydroxyl groups that arise from atmospheric moisture adsorption.[58,59] The EVOH-passivated sample in Figure 7b has a primary peak at 529.54 eV and a broad secondary peak at 531.70 eV, arising from the O−Zn bond and −OH groups, respectively. Secondary peaks in core level O 1s are often ascribed to oxygen vacancies, although there is recent evidence by Frankcombe and Liu[58] that suggests little evidence of oxygen defects in the bulk region of ZnO and more likely to be due to interaction of the hydroxyl from H_2O or surface oxygen on the ZnO surface. As such, the secondary peak at higher binding energies of 531.56 eV for the nonpassivated sample and 531.70 eV for the EVOH-passivated sample is interpreted as −OH groups, with a characteristic binding energy 1−2 eV higher than that of the O−Zn bond. The atomic ratio of O−Zn to −OH on the measured surface is 40.8% O−Zn to 59.2% −OH for the nonpassivated sample versus 55.4% O−Zn to 44.6% −OH for the EVOH-passivated one. This indicates a reduction in the concentration of −OH groups, surface O_2^-, and H_2O in the EVOH-passivated sample and demonstrates the effectiveness of simultaneous UV-vacuum-heat treatment.

The TLM results are summarized in Figure 8 with the full data sets being supplied in the Supporting Information. Figure 8a shows the sheet resistance of the different passivation methods when processed under UV-vacuum conditions. Water passivation reduced the ZnO sheet resistivity by approximately 10^3 times compared to the unpassivated ZnO NP, which is consistent with chemical changes in eqs 4−7. The use of the UV-vacuum-water process increases the condensation of the water vapor on the surface of the ZnO NP film, leading to a lower sheet resistance compared to that of Vidor et al.,[38] in which their ZnO was processed at atmospheric pressure. Notably, the TLM results for the two polymer passivation layers yielded similar results, reducing the resistance by approximately 5×10^5 times, which is consistent with results from the interdigitated devices shown in Table 1. In contrast, for the water-passivated ZnO NP film, the TLM results do not agree with the interdigitated device due to the timing of the measurements. The interdigitated device was measured immediately after processing, whereas the TLM structure was measured 1 h after the UV-vacuum-water process. The delay in the TLM measurement causes readsorption of oxygen, increasing the ZnO NP sheet resistance. The UV-vacuum-water process has a greater oxygen permeability through the polymer layers, which leads to a higher initial sheet resistance. Figure 8b shows the contact resistance of the as-deposited, UV-vacuum-water-treated ZnO NPs and EVA- and EVOH-passivated ZnO NPs. A consistent transfer length of 0.05 mm extracted from the TLM results for all ZnO NP-passivated films indicates a reliable ohmic contact between the solution-processed ZnO NPs and the silver electrodes. These contacts are unaffected by the passivation materials or the UV-vacuum treatment process.

Regarding the ZnO NP film's long-term electrical stability investigation, the electron carrier concentration of the EVA-passivated ZnO NP film reduces to a stable level after 4 days. This is due to the higher level of oxygen permeability of EVA compared with EVOH (the oxygen transmission rate of EVA is 180 cm^3 mm/m^2 day atm,[43] while the rate of EVOH is 0.1 cm^3 mm/m^2 day atm[43]). Also, the bond between the ZnO film and EVA is not as strong as that for EVOH due to the different processing methods with EVA being applied as a dry film and then heated to 190 °C. The hydroxyl functional groups in EVOH enable a much stronger bond to the ZnO surface and contribute to the lower sheet resistance of the EVOH-passivated ZnO NP films.

As shown in Table 1, upon re-exposure to UV light after 60 days, the resistivity of ZnO NPs passivated by EVA remained lower than that of unpassivated films when measured 1 min after re-exposure. This indicates that the oxygen molecules are very quickly readsorbed on the surface of the unpassivated films, whereas EVA does slow down the reabsorption process.

https://doi.org/10.1021/acsaelm.4c00355
ACS Appl. Electron. Mater. 2024, 6, 4277−4287

Although EVOH significantly reduces oxygen transmission rates, it only limits oxygen migration to the ZnO NP film surface, and its film thickness has a significant impact on its effectiveness. For EVOH films of 10 and 20 μm in thickness, the resistance begins to increase after 2 days, underscoring the inability of these thin layers to provide adequate passivation. The 80 μm-thick EVOH-ZnO device exhibited a minimal resistance increase even after 60 days, demonstrating superior stability. Note that the initial resistance of thicker EVOH-passivated interdigitated ZnO devices tends to be higher. This could be attributed to reduced UV illumination efficacy in removing oxygen molecules from the ZnO surface during passivation. Additionally, the DMSO solvent used in the EVOH solution does etch the ZnO film during the passivation process, resulting in thinner film thicknesses. The thicker EVOH, the longer ZnO is exposed to DMSO before it evaporates, resulting in higher initial resistance compared with thinner EVOH layers.

The conductivity of the film can be influenced by the carrier concentration and mobility. As shown in the SEM image of Figure 3, the porous nature of the ZnO NP film allows the oxygen molecule to incorporate into it, resulting in surface depletion. This effect reduces the carrier concentration and mobility while considerably increasing the film resistivity. The photoresponse of the ZnO NP film can be explained by the following:[60] (i) rapid photogeneration and recombination of electron−hole pairs and (ii) slow adsorption of the oxygen molecule. With the passivation and UV-vacuum-heat process, secondary recombination can be very slow; as a result, the ZnO NP film has a higher carrier concentration and mobility.

The resistivity comparison of different works is shown in Table 2. The resistivity of the solution-processed ZnO NP film is 3 to 5 orders of magnitude higher than that of films deposited using other techniques. Variations in resistivity are further influenced by specific solution and postprocessing methodologies used. The resistivity of the ZnO NP film passivated by EVOH and with the UV-vacuum-heat process shows similar resistivity with the ALD-deposited ZnO film and significantly lower resistivity than that of other deposition methods. The $I-V$ curve of the unpassivated and passivated ZnO NP films on the interdigitated silver electrode is shown in the Supporting Information (Figures S8−S10). The as-deposited ZnO NP film exhibits high resistivity and hysteresis, and the EVOH-passivated ZnO NP film without the UV-vacuum-heat process shows a low current level but no significant hysteresis. The passivated ZnO NP film fabricated with the UV-vacuum-heat process shows a significantly higher current level and lower hysteresis.

Table 2. Comparison of ZnO Films Deposited by Different Methods

Deposition method	Sheet resistance (Ω/□)	Thickness (nm)	Resistivity (Ω·cm)
ALD[61]	1.6×10^5	80	1.25
Atmospheric pressure chemical vapor deposition[62]	1.8×10^7	300	2,460
Solution-processed ZnO with N_2 annealed[63]	9.9×10^8	100	9,900
Solution-processed ZnO with O_2 annealed[63]	3.8×10^{10}	100	380,000
Inkjet-printed ZnO[64]	5.0×10^9	81	40,500
Sputtering ZnO[65]	2.0×10^9	50	10,000
ZnO in this work with EVOH passivation	2.5×10^4	2350	5.80

4. CONCLUSIONS

This paper has demonstrated a novel fabrication method that enhances the electrical properties of the solution-processed ZnO NP film using UV exposure and by heating the sample in a vacuum environment. This method has reduced the resistance of the solution-processed ZnO NP film to levels comparable with those of chemical or physical vapor-deposited films. This enhancement can achieve long-term stability with a solution-processed EVOH passivation layer of 80 μm in thickness. The fabrication method proposed in this paper can initially minimize the influence of oxygen on ZnO NP and slow down any subsequent adsorption effect. In the comparison of the two passivation materials (EVA and EVOH), it can be concluded that it is beneficial for any passivating polymer to have hydroxyl functional groups to bond closely to the ZnO surface and contribute to the reduction in resistance. The oxygen transmission rate through the passivation layer could be further improved by adding inorganic materials that have lower oxygen transmission rates. The inclusion of glass flakes or nanoparticles, for example, would make the path where the oxygen molecules travel much longer. The addition of such materials will, however, alter the mechanical properties of the passivating film. Solution processing is inexpensive, and the materials used are environmentally sustainable. ZnO films are widely used to monitor UV and as a chemical sensor to detect reducing substances. One drawback of using the thick EVOH passivation layer is the reduced sensitivity to these measurements, and EVA passivation may be better suited to photoresistor applications. Low-resistivity solution-processed ZnO NPs can be particularly sensitive to substances that dissociate due to hydrogen bonding, making them suitable for use in biochemical sensors and field effect transistors.

■ ASSOCIATED CONTENT

Supporting Information

The Supporting Information is available free of charge at https://pubs.acs.org/doi/10.1021/acsaelm.4c00355.

Contains the data of transfer length method (TLM), time-dependent resistance change of interdigitated devices with different passivation, and X-ray photoelectron spectroscopy of ZnO NP films (PDF)

■ AUTHOR INFORMATION

Corresponding Author

Mengyang Qu − *School of Electronics and Computer Science, University of Southampton, Southampton SO17 1BJ, United Kingdom*; orcid.org/0009-0003-3685-8658; Email: mq1g19@soton.ac.uk

Authors

Sheng Yong − *School of Electronics and Computer Science, University of Southampton, Southampton SO17 1BJ, United Kingdom*

Ben D. Rowlinson − *School of Electronics and Computer Science, University of Southampton, Southampton SO17 1BJ, United Kingdom*; orcid.org/0000-0002-7533-0579

Amanda A. Green − *School of Electronics and Computer Science, University of Southampton, Southampton SO17 1BJ, United Kingdom*

https://doi.org/10.1021/acsaelm.4c00355
ACS Appl. Electron. Mater. 2024, 6, 4277−4287

Stephen P. Beeby − *School of Electronics and Computer Science, University of Southampton, Southampton SO17 1BJ, United Kingdom*
Harold M. H. Chong − *School of Electronics and Computer Science, University of Southampton, Southampton SO17 1BJ, United Kingdom;* orcid.org/0000-0002-7110-5761
Maurits R. R. de Planque − *School of Electronics and Computer Science, University of Southampton, Southampton SO17 1BJ, United Kingdom*

Complete contact information is available at: https://pubs.acs.org/10.1021/acsaelm.4c00355

Notes

The authors declare no competing financial interest.

■ ACKNOWLEDGMENTS

Professor Steve P. Beeby is supported by RAEng under the Chairs in Emerging Technologies Scheme, and Dr. Ben D. Rowlinson is funded under the Norman Godinho Fellowship. The data for this paper can be found at doi.org/10.5258/SOTON/D3069. The authors are grateful for the support of the Printed Electronics and Materials Laboratory and Southampton Nanofabrication Centre.

■ REFERENCES

(1) Pang, Y.; Li, J.; Zhou, T.; Yang, Z.; Luo, J.; Zhang, L.; Dong, G.; Zhang, C.; Wang, Z. L. Flexible Transparent Tribotronic Transistor for Active Modulation of Conventional Electronics. *Nano Energy* **2017**, *31*, 533−540.
(2) Takahashi, T.; Yu, Z.; Chen, K.; Kiriya, D.; Wang, C.; Takei, K.; Shiraki, H.; Chen, T.; Ma, B.; Javey, A. Carbon Nanotube Active-Matrix Backplanes for Mechanically Flexible Visible Light and X-Ray Imagers. *Nano Lett.* **2013**, *13* (11), 5425−5430.
(3) Luo, N.; Ding, J.; Zhao, N.; Leung, B. H. K.; Poon, C. C. Y. Mobile Health: Design of Flexible and Stretchable Electrophysiological Sensors for Wearable Healthcare Systems. In *2014 11th International Conference on Wearable and Implantable Body Sensor Networks*; 2014; pp 87−91. DOI: 10.1109/BSN.2014.25.
(4) Guo, C.; Yu, Y.; Liu, J. Rapidly Patterning Conductive Components on Skin Substrates as Physiological Testing Devices via Liquid Metal Spraying and Pre-Designed Mask. *J. Mater. Chem. B* **2014**, *2* (35), 5739−5745.
(5) Koo, H.-S.; Pan, P.-C.; Kawai, T.; Chen, M.; Wu, F.-M.; Liu, Y.-T.; Chang, S.-J. Physical Chromaticity of Colorant Resist of Color Filter Prepared by Inkjet Printing Technology. *Appl. Phys. Lett.* **2006**, *88* (11), 111908.
(6) Fitriana; Septiani, N. L. W.; Adhika, D. R.; Saputro, A. G.; Nugraha; Yuliarto, B. Enhanced NO Gas Performance of (002)-Oriented Zinc Oxide Nanostructure Thin Films. *IEEE Access* **2019**, *7*, 155446−155454.
(7) Khan, S.; Ali, S.; Khan, A.; Wang, B.; Bermak, A. Printing Sensors on Biocompatible Substrates for Selective Detection of Glucose. *IEEE Sensors J.* **2021**, *21* (4), 4167−4175.
(8) Khan, S. A.; Saqib, M.; Rehman, M. M.; Mutee Ur Rehman, H. M.; Rahman, S. A.; Yang, Y.; Kim, S.; Kim, W.-Y. A Full-Range Flexible and Printed Humidity Sensor Based on a Solution-Processed P(VDF-TrFE)/Graphene-Flower Composite. *Nanomaterials* **2021**, *11* (8), 1915.
(9) Tong, S.; Sun, J.; Yang, J. Printed Thin-Film Transistors: Research from China. *ACS Appl. Mater. Interfaces* **2018**, *10* (31), 25902−25924.
(10) Marques, G. C.; Birla, A.; Arnal, A.; Dehm, S.; Ramon, E.; Tahoori, M. B.; Aghassi-Hagmann, J. Printed Logic Gates Based on Enhancement- and Depletion-Mode Electrolyte-Gated Transistors. *IEEE Trans. Electron Devices* **2020**, *67* (8), 3146−3151.
(11) Feng, X.; Scholz, A.; Tahoori, M. B.; Aghassi-Hagmann, J. An Inkjet-Printed Full-Wave Rectifier for Low-Voltage Operation Using Electrolyte-Gated Indium-Oxide Thin-Film Transistors. *IEEE Trans. Electron Devices* **2020**, *67* (11), 4918−4923.
(12) John, R. A.; Chien, N. A.; Shukla, S.; Tiwari, N.; Shi, C.; Ing, N. G.; Mathews, N. Low-Temperature Chemical Transformations for High-Performance Solution-Processed Oxide Transistors. *Chem. Mater.* **2016**, *28* (22), 8305−8313.
(13) Kumar, N.; Kumar, J.; Panda, S. Back-Channel Electrolyte-Gated a-IGZO Dual-Gate Thin-Film Transistor for Enhancement of pH Sensitivity Over Nernst Limit. *IEEE Electron Device Lett.* **2016**, *37* (4), 500−503.
(14) Kesorn, P.; Bermundo, J. P.; Yoshida, N.; Nonaka, T.; Fujii, M. N.; Ishikawa, Y.; Uraoka, Y. Low Temperature High-k Solution Processed Hybrid Gate Insulator for High Performance Amorphous In-Ga-Zn-O Thin-Film Transistors. In *2019 26th International Workshop on Active-Matrix Flatpanel Displays and Devices (AM-FPD)*; 2019; Vol. *26*th, pp 1−2. DOI: 10.23919/AM-FPD.2019.8830627.
(15) Becker, T. E.; Vidor, F. F.; Wirth, G. I.; Meyers, T.; Reker, J.; Hilleringmann, U. Time Domain Electrical Characterization in Zinc Oxide Nanoparticle Thin-Film Transistors. In *2018 IEEE 19th Latin-American Test Symposium (LATS)*; 2018; pp 1−6. DOI: 10.1109/LATW.2018.8349695.
(16) Carvalho, J.; Dubceac, V.; Grey, P.; Cunha, I.; Fortunato, E.; Martins, R.; Clausner, A.; Zschech, E.; Pereira, L. Fully Printed Zinc Oxide Electrolyte-Gated Transistors on Paper. *Nanomaterials* **2019**, *9* (2), 169.
(17) Kaufmann, I. R.; Zerey, O.; Meyers, T.; Reker, J.; Vidor, F.; Hilleringmann, U. A Study about Schottky Barrier Height and Ideality Factor in Thin Film Transistors with Metal/Zinc Oxide Nanoparticles Structures Aiming Flexible Electronics Application. *Nanomaterials* **2021**, *11* (5), 1188.
(18) Basu, P. K.; Saha, N.; Maji, S.; Saha, H.; Basu, S. Nanoporous ZnO Thin Films Deposited by Electrochemical Anodization: Effect of UV Light. *J. Mater. Sci: Mater. Electron* **2008**, *19* (6), 493−499.
(19) Wan, L.; He, F.; Qin, Y.; Lin, Z.; Su, J.; Chang, J.; Hao, Y. Effects of Interfacial Passivation on the Electrical Performance, Stability, and Contact Properties of Solution Process Based ZnO Thin Film Transistors. *Materials* **2018**, *11* (9), 1761.
(20) Seo, S.-J.; Yang, S.; Ko, J.-H.; Bae, B.-S. Effects of Sol-Gel Organic-Inorganic Hybrid Passivation on Stability of Solution-Processed Zinc Tin Oxide Thin Film Transistors. *Electrochem. Solid-State Lett.* **2011**, *14* (9), H375.
(21) Rasheed, F.; Rommel, M.; Marques, G. C.; Wenzel, W.; Tahoori, M. B.; Aghassi-Hagmann, J. Channel Geometry Scaling Effect in Printed Inorganic Electrolyte-Gated Transistors. *IEEE Trans. Electron Devices* **2021**, *68* (4), 1866−1871.
(22) Garlapati, S. K.; Mishra, N.; Dehm, S.; Hahn, R.; Kruk, R.; Hahn, H.; Dasgupta, S. Electrolyte-Gated, High Mobility Inorganic Oxide Transistors from Printed Metal Halides. *ACS Appl. Mater. Interfaces* **2013**, *5* (22), 11498−11502.
(23) Verbakel, F.; Meskers, S. C. J.; Janssen, R. A. J. Electronic Memory Effects in Diodes of Zinc Oxide Nanoparticles in a Matrix of Polystyrene or Poly(3-Hexylthiophene). *J. Appl. Phys.* **2007**, *102* (8), No. 083701.
(24) Jin, Y.; Wang, J.; Sun, B.; Blakesley, J. C.; Greenham, N. C. Solution-Processed Ultraviolet Photodetectors Based on Colloidal ZnO Nanoparticles. *Nano Lett.* **2008**, *8* (6), 1649−1653.
(25) Saputro, A. G.; Akbar, F. T.; Setyagar, N. P. P.; Agusta, M. K.; Pramudya, A. D.; Dipojono, H. K. Effect of Surface Defects on the Interaction of the Oxygen Molecule with the ZnO($10\bar{1}0$) Surface. *New J. Chem.* **2020**, *44* (18), 7376−7385.
(26) Franco, M. A.; Conti, P. P.; Andre, R. S.; Correa, D. S. A Review on Chemiresistive ZnO Gas Sensors. *Sensors and Actuators Reports* **2022**, *4*, No. 100100.
(27) Ji, H.; Zeng, W.; Li, Y. Gas Sensing Mechanisms of Metal Oxide Semiconductors: A Focus Review. *Nanoscale* **2019**, *11* (47), 22664−22684.

(28) Pickett, A.; Mohapatra, A. A.; Ray, S.; Lu, Q.; Bian, G.; Ghosh, K.; Patil, S.; Guha, S. UV−Ozone Modified Sol−Gel Processed ZnO for Improved Diketopyrrolopyrrole-Based Hybrid Photodetectors. *ACS Appl. Electron. Mater.* **2019**, *1* (11), 2455−2462.
(29) Park, K.-H.; Han, G. D.; Neoh, K. C.; Kim, T.-S.; Shim, J. H.; Park, H.-D. Antibacterial Activity of the Thin ZnO Film Formed by Atomic Layer Deposition under UV-A Light. *Chemical Engineering Journal* **2017**, *328*, 988−996.
(30) Guo, Y.; Zhou, J.; Ji, Z.; Liu, Y.; Cao, R.; Zhuo, F.; Tan, K.; Duan, H.; Fu, Y. A New Strategy to Minimize Humidity Influences on Acoustic Wave Ultraviolet Sensors Using ZnO Nanowires Wrapped with Hydrophobic Silica Nanoparticles. *Microsyst Nanoeng* **2022**, *8* (1), 1−11.
(31) Yang, P.-H.; Chan, C.-T.; Zhang, Y.-S. ZnO Film Flexible Printed Circuit Board pH Sensor Measurement and Characterization. *IEEE Access* **2022**, *10*, 96091−96099.
(32) Akrofi, J. D.; Ebert, M.; Reynolds, J. D.; Sun, K.; Hu, R.; de Planque, M. R. R.; Chong, H. M. H. Multi-Stack Insulator to Minimise Threshold Voltage Drift in ZnO FET Sensors Operating in Ionic Solutions. *Micro and Nano Engineering* **2020**, *8*, No. 100066.
(33) Kim, D.; Woo, H. K.; Lee, Y. M.; Kim, Y.; Choi, J.-H.; Oh, S. J. Controllable Doping and Passivation of ZnO Thin Films by Surface Chemistry Modification to Design Low-Cost and High-Performance Thin Film Transistors. *Appl. Surf. Sci.* **2020**, *509*, No. 145289.
(34) Wu, P.; Zhang, J.; Lu, J.; Li, X.; Wu, C.; Sun, R.; Feng, L.; Jiang, Q.; Lu, B.; Pan, X.; Ye, Z. Instability Induced by Ultraviolet Light in ZnO Thin-Film Transistors. *IEEE Trans. Electron Devices* **2014**, *61* (5), 1431−1435.
(35) Wei, X.; Kumagai, S.; Sasaki, M.; Watanabe, S.; Takeya, J. Stabilizing Solution-Processed Metal Oxide Thin-Film Transistors via Trilayer Organic−Inorganic Hybrid Passivation. *AIP Advances* **2021**, *11* (3), No. 035027.
(36) Li, Y.; Della Valle, F.; Simonnet, M.; Yamada, I.; Delaunay, J.-J. Competitive Surface Effects of Oxygen and Water on UV Photoresponse of ZnO Nanowires. *Appl. Phys. Lett.* **2009**, *94* (2), No. 023110.
(37) Jacobs, C. B.; Maksov, A. B.; Muckley, E. S.; Collins, L.; Mahjouri-Samani, M.; Ievlev, A.; Rouleau, C. M.; Moon, J.-W.; Graham, D. E.; Sumpter, B. G.; Ivanov, I. N. UV-Activated ZnO Films on a Flexible Substrate for Room Temperature O2 and H2O Sensing. *Sci. Rep* **2017**, *7* (1), 6053.
(38) Vidor, F. F.; Meyers, T.; Hilleringmann, U.; Wirth, G. I. Influence of UV Irradiation and Humidity on a Low-Cost ZnO Nanoparticle TFT for Flexible Electronics. In *2015 IEEE 15th International Conference on Nanotechnology (IEEE-NANO)*; 2015; pp 1179−1181. DOI: 10.1109/NANO.2015.7388836.
(39) Vai, A. T.; Kuznetsov, V. L.; Dilworth, J. R.; Edwards, P. P. UV-Induced Improvement in ZnO Thin Film Conductivity: A New in Situ Approach. *J. Mater. Chem. C* **2014**, *2* (45), 9643−9652.
(40) Huang, H.-D.; Ren, P.-G.; Zhong, G.-J.; Olah, A.; Li, Z.-M.; Baer, E.; Zhu, L. Promising Strategies and New Opportunities for High Barrier Polymer Packaging Films. *Prog. Polym. Sci.* **2023**, *144*, No. 101722.
(41) Morris, B. A. 4 - Commonly Used Resins and Substrates in Flexible Packaging. In *The Science and Technology of Flexible Packaging*; Morris, B. A., Ed.; Plastics Design Library; William Andrew Publishing: Oxford, 2017; pp 69−119. DOI: 10.1016/B978-0-323-24273-8.00004-6.
(42) Siracusa, V. Packaging Material in the Food Industry. In *Antimicrobial Food Packaging*; Elsevier, 2016; pp 95−106. DOI: 10.1016/B978-0-12-800723-5.00007-3.
(43) McKeen, L. W. Polyvinyls and Acrylics. In *Film Properties of Plastics and Elastomers*; Elsevier, 2012; pp 219−254. DOI: 10.1016/B978-1-4557-2551-9.00010-4.
(44) Lee, S. H.; Han, K.-Y.; Chang, H. J. Properties of Passivation Layer Formed by Solution Process on Flexible CIGS Solar Cells. *Mol. Cryst. Liq. Cryst.* **2022**, *734* (1), 47−62.
(45) Jang, J. H.; Kim, B.-J.; Kim, J.; Han, E.; Choi, E. Y.; Ji, C. H.; Kim, K.-T.; Kim, J.; Park, N. A Novel Approach for the Development of Moisture Encapsulation Poly(Vinyl Alcohol-Co-Ethylene) for Perovskite Solar Cells. *ACS Omega* **2019**, *4* (5), 9211−9218.
(46) Yong, S.; Shi, J.; Beeby, S. Wearable Textile Power Module Based on Flexible Ferroelectret and Supercapacitor. *Energy Technology* **2019**, *7* (5), 1800938.
(47) Heo, K.-J.; Tarsoly, G.; Lee, J.-Y.; Choi, S. G.; Koh, J.-H.; Kim, S.-J. Improved Electrical and Temporal Stability of In-Zn Oxide Semiconductor Thin-Film Transistors With Organic Passivation Layer. *IEEE J. Electron Devices Soc.* **2022**, *10*, 660−665.
(48) Postica, V.; Lupan, O.; Gapeeva, A.; Hansen, L.; Khaledialidusti, R.; Mishra, A. K.; Drewes, J.; Kersten, H.; Faupel, F.; Adelung, R.; Hansen, S. Improved Long-Term Stability and Reduced Humidity Effect in Gas Sensing: SiO2 Ultra-Thin Layered ZnO Columnar Films. *Advanced Materials Technologies* **2021**, *6* (5), 2001137.
(49) Zhang, Y.; Chen, Z.; Liu, S.; Xu, Y.-J. Size Effect Induced Activity Enhancement and Anti-Photocorrosion of Reduced Graphene Oxide/ZnO Composites for Degradation of Organic Dyes and Reduction of Cr(VI) in Water. *Applied Catalysis B: Environmental* **2013**, *140−141*, 598−607.
(50) Sebastian, J.; Thachil, E. T.; Mathen, J. J.; Edakkara, A. J.; Kuriakose, N.; Joseph, G. P.; Sebastian, J. Preparation and Characterization of ZnSe/EVA Nanocomposites for Photovoltaic Modules. *JMMCE* **2015**, *03* (04), 215−224.
(51) Kubacka, A.; Cerrada, M. L.; Serrano, C.; Fernández-García, M.; Ferrer, M.; Fernández-Garcia, M. Plasmonic Nanoparticle/Polymer Nanocomposites with Enhanced Photocatalytic Antimicrobial Properties. *J. Phys. Chem. C* **2009**, *113* (21), 9182−9190.
(52) Aleksic, O.; Radojcic, B.; Ramovic, R. Electrode Effect on NTC Planar Thermistor Vol. Resistivity.In *2006 25th International Conference on Microelectronics*; Belgrade, Serbia and Montenegro, IEEE, 2006; pp 580−583. DOI: 10.1109/ICMEL.2006.1651033.
(53) Tyrrell, J. E.; Boutelle, M. G.; Campbell, A. J. Measurement of Electrophysiological Signals In Vitro Using High-Performance Organic Electrochemical Transistors. *Adv. Funct. Mater.* **2021**, *31* (1), 2007086.
(54) Janotti, A.; Van de Walle, C. G. Fundamentals of Zinc Oxide as a Semiconductor. *Rep. Prog. Phys.* **2009**, *72* (12), 126501.
(55) Sanches De Lima, B.; Martínez-Alanis, P. R.; Güell, F.; Dos Santos Silva, W. A.; Bernardi, M. I. B.; Marana, N. L.; Longo, E.; Sambrano, J. R.; Mastelaro, V. R. Experimental and Theoretical Insights into the Structural Disorder and Gas Sensing Properties of ZnO. *ACS Appl. Electron. Mater.* **2021**, *3* (3), 1447−1457.
(56) Liau, L. C.-K.; Lin, Y.-H. Effects of Electric Fields on the Conduction of Polyvinyl Alcohol (PVA)/ZnO Films by Photoluminescence Analysis. *J. Lumin.* **2017**, *181*, 217−222.
(57) Rawal, T. B.; Ozcan, A.; Liu, S.-H.; Pingali, S. V.; Akbilgic, O.; Tetard, L.; O'Neill, H.; Santra, S.; Petridis, L. Interaction of Zinc Oxide Nanoparticles with Water: Implications for Catalytic Activity. *ACS Applied Nano Materials* **2019**. 24257.
(58) Frankcombe, T. J.; Liu, Y. Interpretation of Oxygen 1s X-Ray Photoelectron Spectroscopy of ZnO. *Chem. Mater.* **2023**, *35* (14), 5468−5474.
(59) Tu, Y.; Chen, S.; Li, X.; Gorbaciova, J.; Gillin, W. P.; Krause, S.; Briscoe, J. Control of Oxygen Vacancies in ZnO Nanorods by Annealing and Their Influence on ZnO/PEDOT:PSS Diode Behaviour. *J. Mater. Chem. C* **2018**, *6* (7), 1815−1821.
(60) Wisz, G.; Virt, I.; Sagan, P.; Potera, P.; Yavorskyi, R. Structural, Optical and Electrical Properties of Zinc Oxide Layers Produced by Pulsed Laser Deposition Method. *Nanoscale Res. Lett.* **2017**, *12* (1), 253.
(61) Mohamed, A. H.; Ghazali, N. A. B.; Chong, H. M. H.; Cobley, R. J.; Li, L.; Kalna, K. Channel Mobility and Contact Resistance in Scaled ZnO Thin-Film Transistors. *Solid-State Electron.* **2020**, *172*, No. 107867.
(62) Najafi, N.; Rozati, S. M. Resistivity Reduction of Nanostructured Undoped Zinc Oxide Thin Films for Ag/ZnO Bilayers Using APCVD and Sputtering Techniques. *Mater. Res.* **2018**, *21*, No. e20170933, DOI: 10.1590/1980-5373-mr-2017-0933.

(63) Oura, K.; Wada, H.; Koyama, M.; Maemoto, T.; Sasa, S. Improved Electrical Performance of Solution-Processed Zinc Oxide-Based Thin-Film Transistors with Bilayer Structures. *Journal of Information Display* **2022**, *23* (1), 105−113.
(64) Liu, X.; Wegener, M.; Polster, S.; Jank, M. P. M.; Roosen, A.; Frey, L. Materials Integration for Printed Zinc Oxide Thin-Film Transistors: Engineering of a Fully-Printed Semiconductor/Contact Scheme. *Journal of Display Technology* **2016**, *12* (3), 214−218.
(65) Yang, J.; Hu, L.; Shen, L.; Wang, J.; Cheng, P.; Lu, H.; Zhuge, F.; Ye, Z. Optically Driven Intelligent Computing with ZnO Memristor. *Fundam. Res.* **2022**, *4*, 158.

https://doi.org/10.1021/acsaelm.4c00355
ACS Appl. Electron. Mater. 2024, 6, 4277−4287